J. Fluid Mech. (1986), *vol.* 165, *pp.* 335–353
Printed in Great Britain

Hot-wire-anemometer study of the entry flow in a curved duct

By A. KLUWICK
Institut für Strömungslehre und Wärmeübertragung, Technische Universität Wien, Wiedner Hauptstraße 7, A 1040 Vienna, Austria

AND H. WOHLFAHRT
Höhere Technische Bundeslehranstalt Wiener Neustadt, Dr. Eckenergasse 2-10, A 2700 Wieder Neustadt, Austria

(Received 4 January 1984 and in revised form 20 March 1985)

Experimental results for the axial velocity distribution in the entry region of weakly curved circular ducts at high Dean numbers are presented. Estimates for the displacement thickness of the boundary layer and the wall shear stress obtained from these data are compared with theoretical predictions.

1. Introduction

Fully developed flows in curved ducts have been studied extensively in the past, both theoretically and experimentally. In contrast, much less is known about the flow properties in the entry region and in particular, as expressed in the recent review article of Berger & Talbot (1983), 'the nature of the developing flow in curved pipes for large Dean numbers is far from understood'.

The first theoretical investigations of the flow structure in the entry region were carried out by Singh (1974) and Yao & Berger (1975). Treating the boundary layer as a slightly perturbed Blasius boundary layer, Singh was able to predict a crossover of the maximum axial wall shear from the inner to the outer bend. Likewise, the analysis yields a crossover of the maximum value of the boundary-layer displacement thickness from the outer to the inner bend. If an entry condition of constant dynamic pressure is imposed these crossover phenomena occur at distances which are 1.92 and 1.53 times the radius of the tube respectively.

More recent theoretical work by Weiss (1976), Stewartson, Cebeci & Chang (1980), Kluwick & Wohlfahrt (1984), Yeung (1980) and Holt & Yeung (1983) has yielded additional information about developing flows. In particular, the investigations of Kluwick & Wohlfahrt (1984), Stewartson *et al.* (1980) and Weiss (1976) imposing again the entry condition of constant dynamic pressure, indicate that the boundary-layer thickness and the axial wall shear at the outer bend approach constant values for $x_0 \to \infty$, where x_0 denotes a stretched distance from the entrance of the duct (see (2)). At the inner bend, however, the boundary-layer calculations come to an end at a finite value x_{0s} of x_0. As the critical value x_{0s} is approached, the axial wall shear tends to zero in a singular fashion while the boundary-layer thickness becomes infinite.

Experimental investigations of the flow inside curved circular pipes, including the entry region, have been performed by Agrawal, Talbot & Gong (1978) and Choi, Talbot & Cornet (1979). While in the former study velocity profiles in planes almost parallel to the plane of symmetry were measured by means of laser anemometry, an

electrochemical method was applied in the latter to determine the wall-shear rates. Most recently, Olson & Snyder (1985) have measured axial and transverse velocity profiles in the first 180° of bend in tightly curved pipes.

The experimental studies mentioned above have contributed substantially to the understanding of the formation of fully developed flows in curved circular pipes. However, further experimental data are necessary for a detailed comparison with the results of classical boundary-layer theory presented in Kluwick & Wohlfahrt (1984), Stewartson *et al.* (1980) and Weiss (1976). As an important first step the resolution of the wall-shear-stress distribution along the inner bend of a curved duct has been improved by Talbot & Wong (1982). In contrast, it is the aim of the present investigation to provide additional information about the axial velocity distribution inside the boundary layer and the core region. Since the results given in Kluwick & Wohlfahrt (1984), Stewartson *et al.* (1980) and Weiss (1976) are asymptotic in the sense that the limit of infinite Dean number is considered, our experiments have been carried out at substantially higher values of the Dean number than in previous studies.

2. Experimental apparatus

A schematic representation of the experimental set-up using air as the flow medium is shown in figure 1. Its main parts are the inlet region 1–4, the circular test pipe 5, the radial fan 9 and the throttle 11. The inlet region consisting of the inlet ring 1, the damping screen 2, the honeycomb 3 and the contraction section 4 was carefully designed to produce a laminar and almost uniform stream. Preliminary experiments indicated that the variation of the axial velocity component inside the core was less than $\pm 1\,\%$.

Only the inner part of the oncoming stream enters the thin-walled test pipe 6, while the outer part flows through the annulus between 6 and the outer pipe 5. The test pipe was made from Polyester with a laminated wooden core, the cross-sections of which deviated by less than about $\pm 1\,\%$ from the exact circular shape. In order to obtain a (negligibly) thin boundary layer in the inlet section of the test pipe its wall was sharpened symmetricaly. The radius $\tilde{\xi}_0$ of the test pipe and the radius $\tilde{R}_1$ of the pipe axis were 50 mm and 500 mm respectively, corresponding to the non-dimensional curvature ratio $K_0 = \tilde{\xi}_0/\tilde{R}_1 = 0.1$.

By means of the throttle 11 the velocity U_0 of the fluid in the centre of the inlet section could be varied continuously between 0.5 m s^{-1} and 8.0 m s^{-1} without any apparent instabilities of the radial fan. Experiments were performed at four different values of the Dean number D: 971, 1502, 2021 and 2527, being substantially higher than those investigated in Agrawal *et al.* (1978) and Choi *et al.* (1979). The corresponding values of the Reynolds number are Re: 3070, 4750, 6390 and 7990. Here D and Re are defined in the same way as in Kluwick & Wolhfahrt (1984) and Stewartson *et al.* (1980):

$$Re = \frac{\tilde{U}_0 \tilde{\xi}_0}{\tilde{\nu}}, \quad D = \left(\frac{\tilde{\xi}_0}{\tilde{R}_1}\right)^{\frac{1}{2}} Re = K_0^{\frac{1}{2}}\, Re, \tag{1}$$

where $\tilde{U}_0$ and $\tilde{\nu}$ denote the mean velocity and the kinematic viscosity respectively.

Figure 2 shows a close-up of the test pipe including the coordinate system. Here ϑ, $\tilde{y}$ and φ are respectively the polar angle as measured from the inlet, the distance normal to the wall and the angle measured from the plane of symmetry.

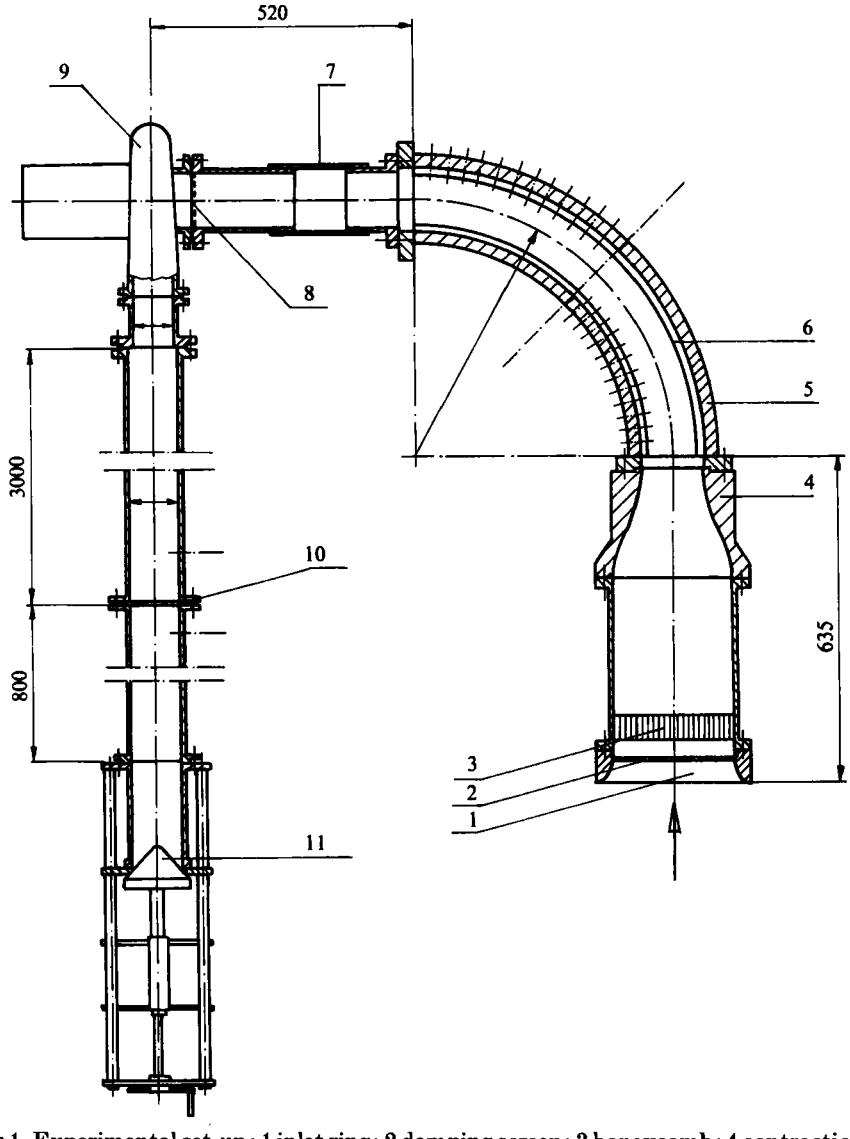

FIGURE 1. Experimental set-up: 1 inlet ring; 2 damping screen; 3 honeycomb; 4 contraction section; 5 outer pipe; 6 test pipe; 7 flexible tube; 8 protective grid; 9 radial fan; 10 orifice assembly; 11 throttle. Distances measured in mm.

The length $\tilde{l}$ is the distance along the pipe axis. In place of ϑ and $\tilde{l}$ the non-dimensional quantities

$$x_0 = \vartheta \left(\frac{1+K_0}{K_0}\right)^{\frac{1}{2}}, \quad l = \frac{\tilde{l}}{\tilde{\xi}_0} \tag{2}$$

as defined in Kluwick & Wolhfahrt (1984) will be used in the following sections.

3. Velocity measurements

Axial-velocity measurements were performed in 12 sections of the test pipe, figure 2, characterized by equal increments $\Delta x_0 = 0.2$ using hot-wire anemometry. At each section four holes were equispaced around one quarter of the circumference as shown

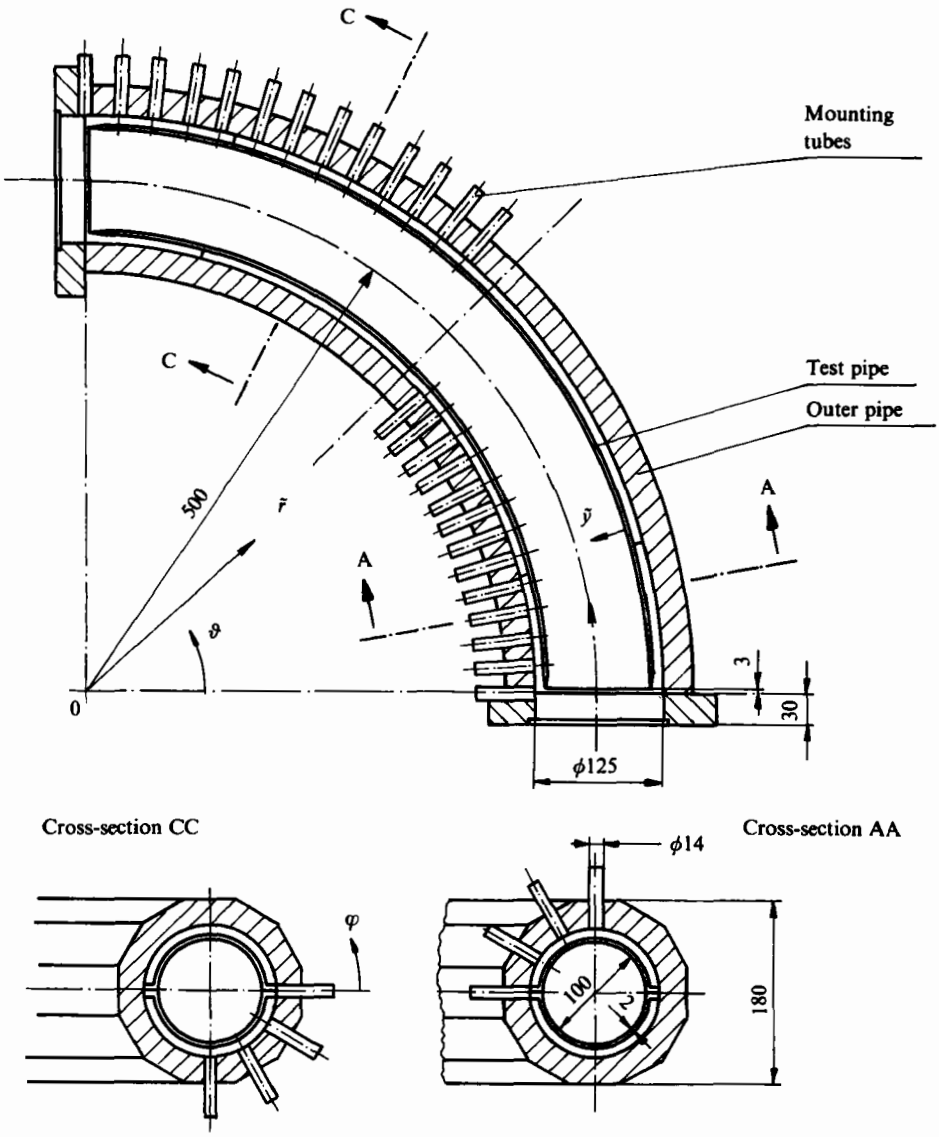

FIGURE 2. Experimental set-up: curved pipe with $K_0 = 0.1$. Distances measured in mm.

in figures 2 and 3. By insertion of the probe through one of these holes such that the hot wire was perpendicular to the axial direction, the velocity profiles inside the boundary layer adjacent to the opposite wall could be determined. Flow measurements for one fixed value of x_0 therefore, had to be performed in two steps. First, velocity profiles were measured for $\varphi = 0$, $\frac{1}{6}\pi$, $\frac{1}{3}\pi$ and $\frac{1}{2}\pi$. Then the test pipe was rotated as a whole and the measurements were completed by recording velocity profiles for $\varphi = \frac{1}{2}\pi$, $\frac{2}{3}\pi$, $\frac{5}{3}\pi$ and π. Comparison of the results for $\frac{1}{2}\pi$ obtained from two different positions of the test pipe showed complete agreement within measuring accuracy.

A DISA model 55K anemometer was used with a miniature probe 55 P 14, a CTA-bridge 55 K 10 and a linearizer 55 K 20. The probe was calibrated by means of a DISA 55 D 90 calibration unit using the 120 mm^2 nozzle.

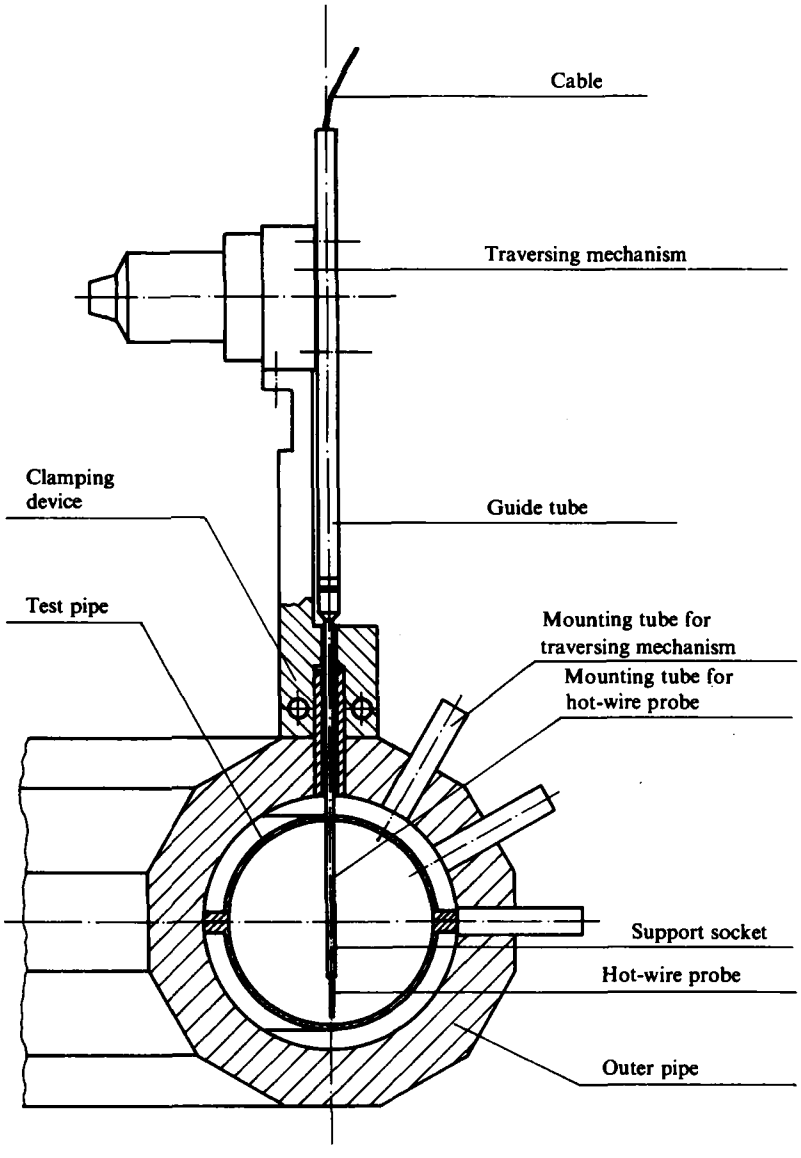

FIGURE 3. Traversing mechanism.

In order to estimate the influence of crossflow on the measurement of the axial velocity the angular response curves of the probe were also determined. The results showed that the normal velocity component was recorded by the probe with an error of less than 3 % provided that the angle between the velocity vector and the direction perpendicular to the hot wire was less than 50°. In agreement with theoretical predictions (Kluwick & Wohlfahrt 1984; Singh 1974), preliminary test runs indicated that the direction of the streamlines deviated from the axial direction by less than this amount in the whole region under consideration. The influence of the secondary-flow velocity on the measurement of the axial velocity may thus be neglected.

Evaluation of the hot-wire signals indicated that, except for the highest value of the Dean number, the boundary layer was laminar over the whole test section. In

the case of $D = 2527$ turbulent fluctuations were first observed on the outer bend at $x_0 = 1.52$.

4. Measurement of the wall distance

A standard traversing mechanism DISA 55 E 40 was used to determine the position of the hot-wire probe relative to the wall of the test pipe. To this end the traversing mechanism was attached to short mounting tubes by means of a specially designed clamping device as depicted in figure 3.

In order to avoid the destruction of the hot wire through contact with the wall of the test pipe the proble was used with a protective pin. With the inlet 1–4 of the experimental set-up removed the probe was then inserted through the tubes until the protective pin was seen to touch the wall. This position was determined with an accuracy of about ± 0.05 mm and served as the reference position of the probe. By continuously increasing the wall distance with the aid of the traversing mechanism the complete velocity profile was obtained and plotted by means of a two-channel recorder. Depending on the boundary-layer thickness at the point under consideration three different scales, 1 cm corresponding to 0.2 mm, 1 cm to 0.5 m and 1 cm to 1 mm were used. For measurements inside the inviscid core the scale 1 cm corresponding to 5 mm proved sufficient.

As an example of the velocity plots obtained, figures 4 (a, b) show the distribution of the streamwise velocity component inside the boundary layer (a) and the core region (b) at $x_0 = 0.92$, $\varphi = \pi$ (inner bend) for the four values of the Reynolds number.

The time needed to determine such a single set of velocity profiles was about 15 min and during this short period of time the effects of slowly changing atmospheric pressure and laboratory temperature on the measurements were negligibly small. However, it took several weeks to complete the test programme. Thus special care was taken to ensure that all measurements were carried out at exactly the same values of the Reynolds numbers. As a consequence different sets of velocity plots exhibit slightly different values of the mean velocity, which reflect the changes of the atmospheric conditions over this extended period of time.

In order to simplify the comparison between experimental and theoretical results the experimental data will be presented in non-dimensional form. The reader interested in the complete set of the original velocity plots is referred to Wohlfahrt (1981).

5. Results

5.1. *The core region*

The measurements indicate that, for the Dean number range $D \gg 1$ under consideration, the velocity distribution inside the core region can be approximated very well by that of a potential vortex

$$\tilde{r}\tilde{U} = \frac{\tilde{\Gamma}}{2\pi} \tag{3}$$

in all test planes. Here $\tilde{r}$ denotes the distance from the centre 0, figure 2.

As a typical example, table 1 summarizes values of $\tilde{r}\tilde{U}$ for $x_0 = 0.92$, $\varphi = \pi$ and $Re = 7990$ corresponding to different wall distances $\tilde{y}$. Owing to displacement effects exerted by the boundary layer on the fluid inside the core region the quantity $\tilde{\Gamma}$ in (3) was found to increase slowly with x_0.

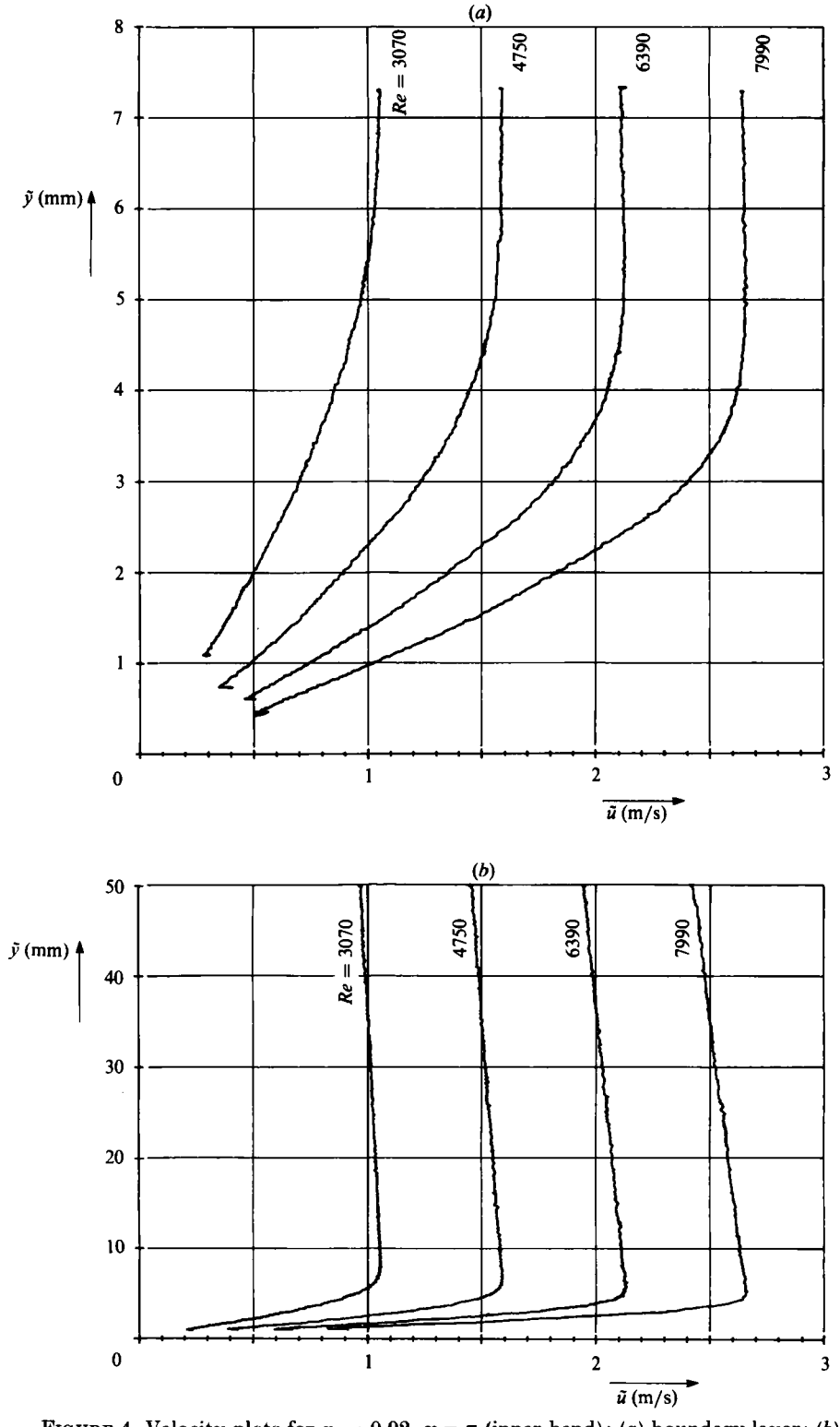

FIGURE 4. Velocity plots for $x_0 = 0.92$, $\varphi = \pi$ (inner bend): (*a*) boundary layer; (*b*) inviscid core.

$\tilde{U}$ m/s	$\tilde{r}$ m	$\tilde{y}$ mm	$\tilde{r}\tilde{U}$ m²/s
2.420	0.50	50	1.210
2.475	0.49	40	1.213
2.525	0.48	30	1.212
2.578	0.47	20	1.212
2.628	0.46	10	1.209

TABLE 1. Variation of $\tilde{r}\tilde{U}$ with $\tilde{y}$ for $x_0 = 0.92$, $\varphi = \pi$ and $Re = 7990$

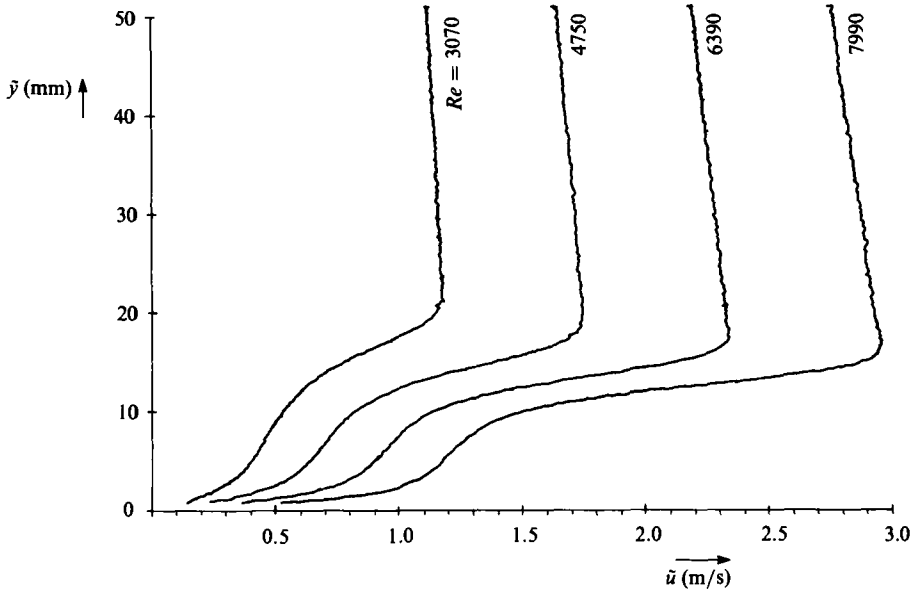

FIGURE 5. Measured profiles of the velocity component $\tilde{u}$ for $K_0 = 0.1$, $x_0 = 2.12$, $\varphi = \pi$ (inner bend), $\tilde{\nu} = 15.25 \times 10^{-6}$ m²/s.

Velocity profiles of the form given by (3) were already present in the first test plane and could be followed downstream to surprisingly large distances where the boundary-layer thickness along the inner bend is no longer small compared with the radius $\tilde{\xi}_0$ of the pipe, figures 5, 7, 8. A similar behaviour of the core flow has been suggested also by Choi *et al.* (1979) on the basis of their measurements of the wall-shear rates.

5.2. *The boundary-layer region*

Since the velocity distribution inside the core region deviates only slightly from that of a potential vortex it is convenient to non-dimensionalize the axial velocity component $\tilde{u}$ and the distance from the wall $\tilde{y}$ by

$$\tilde{U}_r(\varphi, \vartheta) = \frac{\tilde{U}_a(\vartheta)}{1 + K_0 \cos\varphi} \tag{4}$$

and $\tilde{\xi}_0$ respectively:

$$u = \frac{\tilde{u}}{\tilde{U}_r}, \quad y = \frac{\tilde{y}}{\tilde{\xi}_0}. \tag{5}$$

Here $\tilde{U}_a(\vartheta)$ denotes the velocity at the axis of the pipe.

Figures 6(*a–g*) summarize some of the results obtained for $Re = 3070$. Initially, the boundary-layer thickness increases rapidly with increasing values of x_0. Furthermore, for $0 \leqslant \varphi \leqslant \frac{5}{3}\pi$ the growth rate of the boundary-layer thickness is seen to decrease throughout the region under consideration. The decay of the growth rate is most pronounced along the outer bend where the axial velocity profiles for $x_0 = 1.12$, 1.32 and 1.52 are virtually indistinguishable (figure 6*a*). Along the inner bend, however, the initial decay of the growth rate is followed by an increase leading to a rapid thickening of the boundary layer for large values of x_0 (figures 6*g* and 7).

While the results for $0 \leqslant \varphi \leqslant \frac{5}{3}\pi$ show that the velocity profiles preserve their shapes qualitatively for all values of x_0 considered, this is not the case for $\varphi = \pi$. Again, the velocity distributions closely resemble Blasius profiles for $x_0 \ll 1$. Downstream of the singularity as predicted by classical boundary-layer theory (Weiss 1976; Stewartson *et al.* 1980; Kluwick & Wohlfahrt 1984) however, the velocity profiles exhibit two inflexion points. These inflexion points are just visible in figure 6(*g*), $x_0 = 1.32$, but can be seen more clearly in figures 7 and 8 which show the evolution of the velocity profile along the inner bend up to larger distances $x_0 = 2.12$. As expected, the wall slope decreases initially owing to the thickening of the boundary layer. Once the inflexion point has developed, however, this tendency slows down as can be seen from figures 7 and 8. Furthermore, figure 8 indicates that the wall slope will eventually start to increase again in agreement with the wall-shear distributions measured by Talbot & Wong (1982). Finally, it should be noted that the shapes of the velocity profiles at $x_0 = 1.72$ and 2.12 are nearly identical in the outer part of the boundary layer, as if the flow here were lifted up almost passively due to displacement effects caused by the secondary-flow motion directed towards the inner bend.

Although the trend of the wall slope of the velocity profiles in figures 7 and 8 is qualitatively in agreement with the theoretical predictions of Stewartson *et al.* (1980) and Kluwick & Wohlfahrt (1984) the experimental data do not indicate that the streamwise component of the wall stress actually vanishes at some distance from the inlet.

The experimental results obtained for the higher values of the Reynolds number, $Re = 4750$, 6390 and 7990, are qualitatively similar to those for $Re = 3070$, Wohlfahrt (1981), and are thus not presented here in detail. For comparison with figure 7 the velocity profiles measured along the inner bend for $Re = 7990$ are depicted in figure 8.

6. Comparison with theory

The variation of the non-dimensional displacement thickness

$$\delta_u^* = \int_0^\infty (1-u)\,\mathrm{d}y, \quad \delta_u^* = \frac{\delta_u^*}{\xi_0}, \tag{6}$$

with x_0 along various lines $\varphi = \text{const.}$ is depicted in figure 9. Initially δ_u^* increases most rapidly along the outer bend where the velocity in the inviscid core region assumes its smallest value. With increasing distance x_0, however, more and more fluid is drawn towards the inner bend owing to the secondary-flow motion, thus causing the boundary layer there to thicken more rapidly than along all other lines $\varphi = \text{const.} < \pi$. Finally for $x_0 \gtrsim 0.52$ the displacement thickness is largest along the inner bend. The position of the crossover point for δ_u^* is in good agreement with theoretical results, yielding $x_0 = 0.51$ (Singh 1974) and $x_0 = 0.53$ (Kluwick & Wohlfahrt 1984; Wohlfahrt 1981) for $K_0 = 0.1$ respectively. In addition, as predicted by theory, the value of δ_u^* at this point is independent of φ.

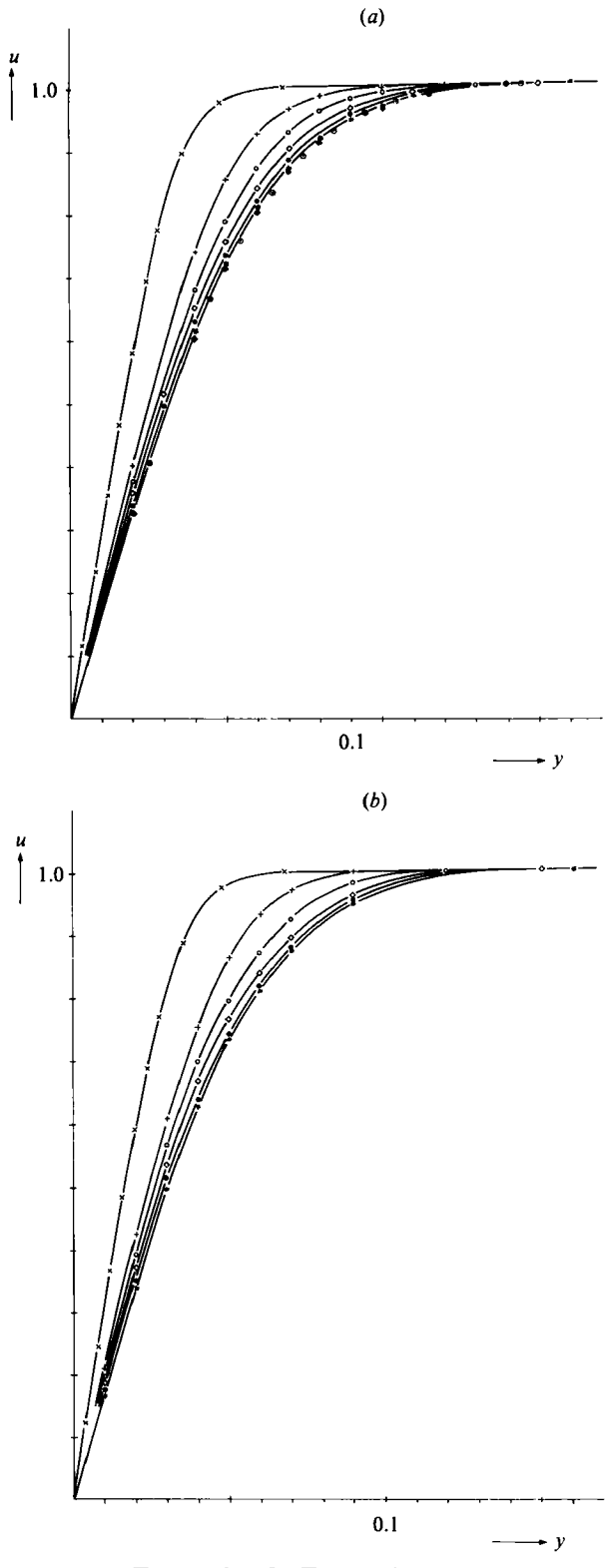

FIGURE 6 (a,b). For caption see p. 347.

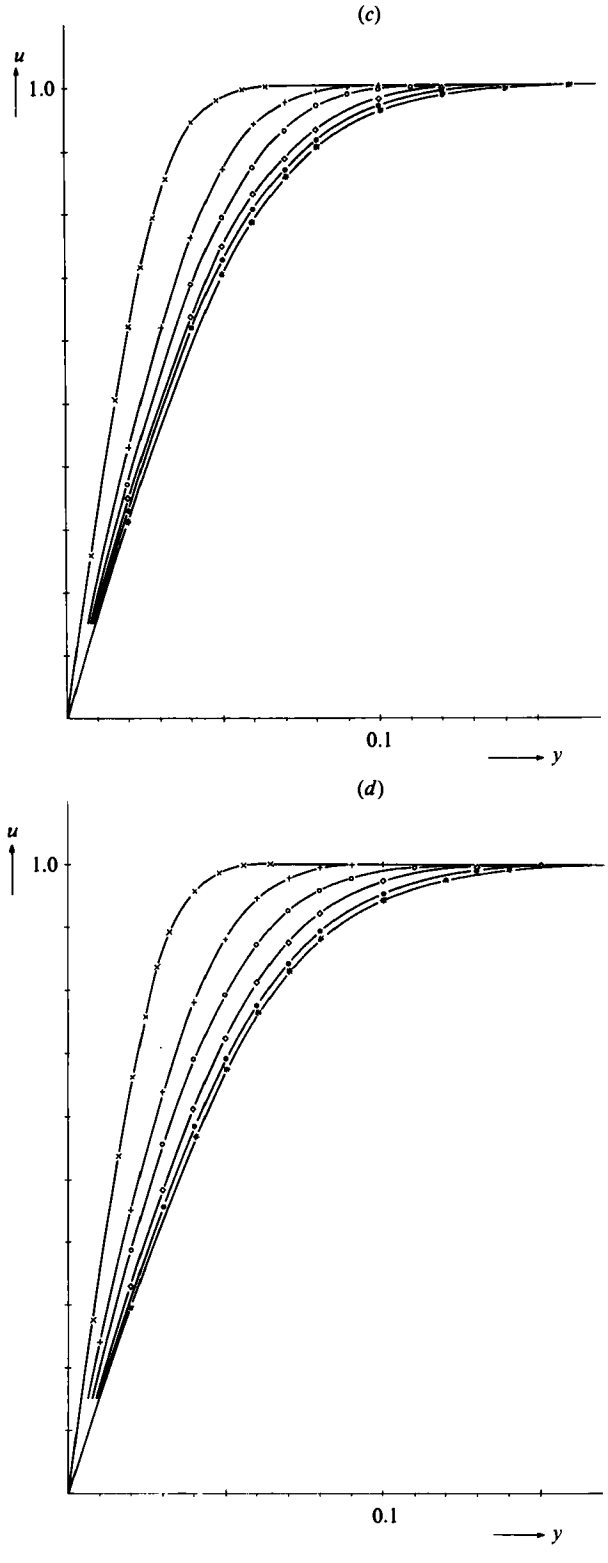

FIGURE 6 (*c*, *d*). For caption see p. 347.

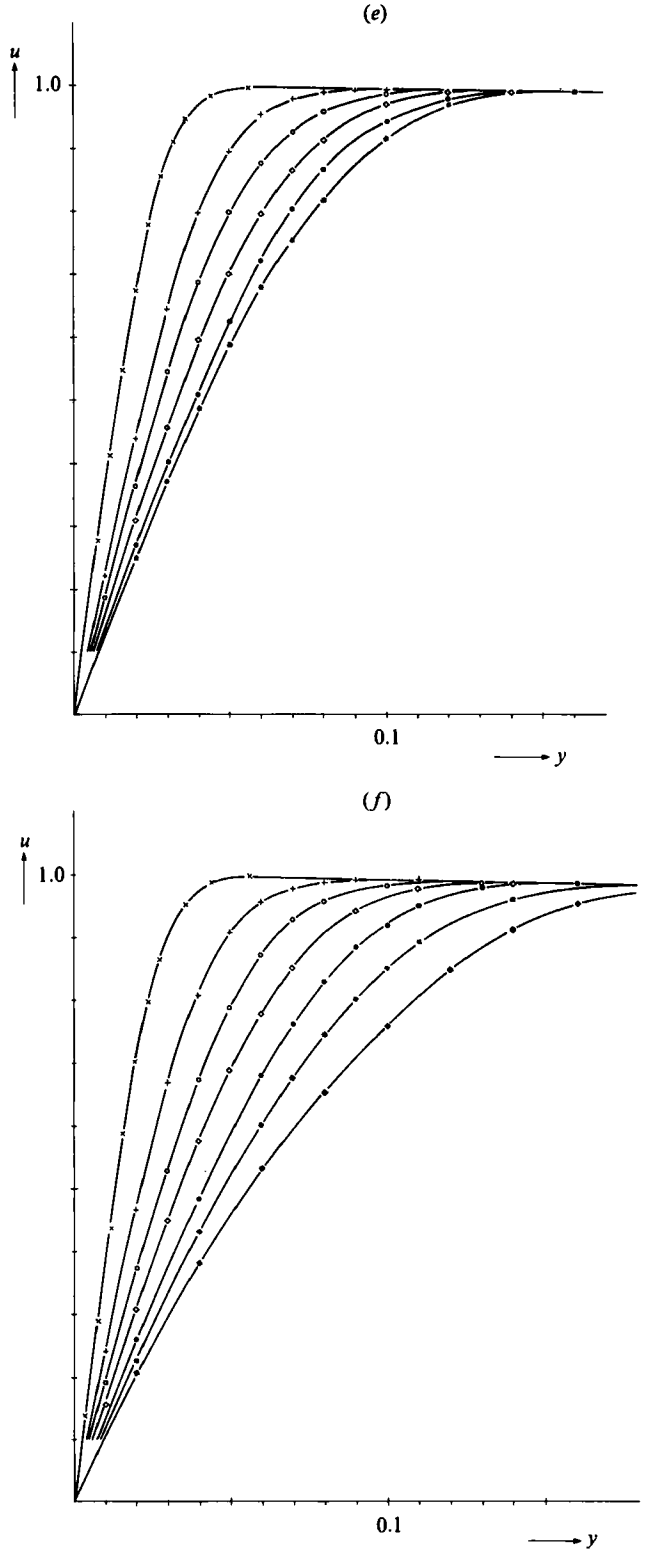

FIGURE 6 (*e,f*). For caption see p. 347.

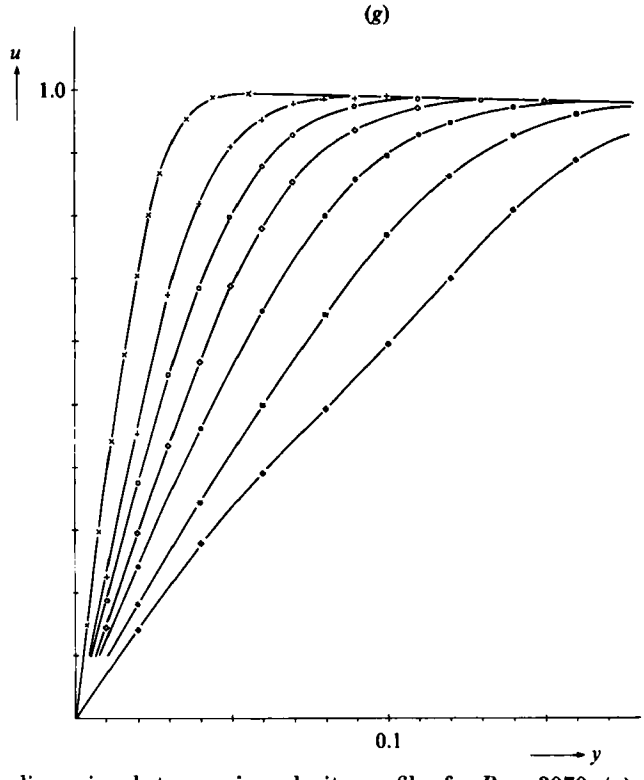

FIGURE 6. Non-dimensional streamwise velocity profiles for $Re = 3070$: (*a*) $\varphi = 0$ (outer bend); (*b*) $\frac{1}{6}\pi$; (*c*) $\frac{1}{3}\pi$; (*d*) $\frac{1}{2}\pi$; (*e*) $\frac{2}{3}\pi$; (*f*) $\frac{5}{6}\pi$; (*g*) π. (inner bend); ×, $x_0 = 0.12$; +, 0.32; ○, 0.52; ◇, 0.72; ●, 0.92; *, 1.12; ◆, 1.32; ⊙, 1.52.

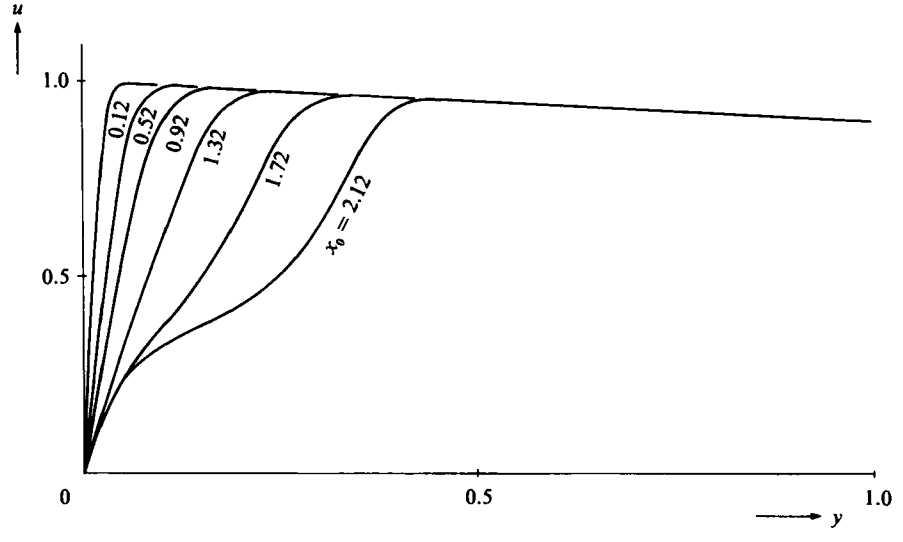

FIGURE 7. Evolution of the streamwise velocity profiles along the inner bend up to $x_0 = 2.12$ for $Re = 3070$.

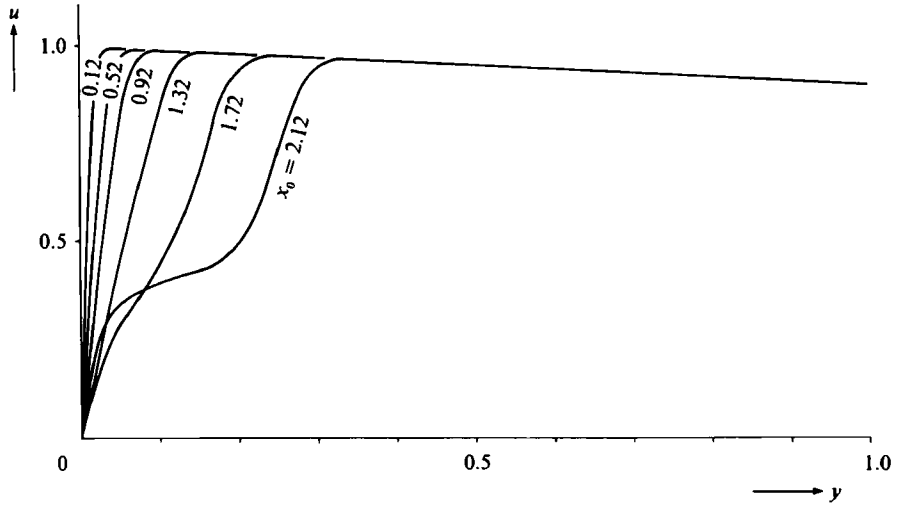

FIGURE 8. Evolution of the streamwise velocity profiles along the inner bend up to $x_0 = 2.12$ for $Re = 7990$.

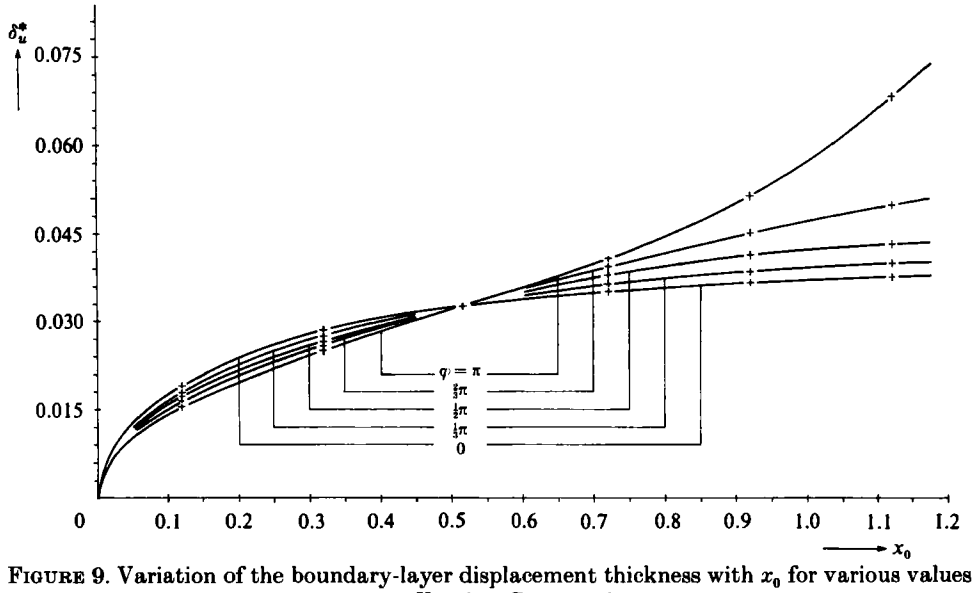

FIGURE 9. Variation of the boundary-layer displacement thickness with x_0 for various values of φ, $K = 0.1$, $Re = 3070$.

Further comparison between the calculated and measured values of the boundary-layer thickness shows that δ_u^* is overpredicted by the first-order theory of Wohlfahrt (1981) for all test planes, a typical value of the magnitude of the error being about 20 % for the lower value of $Re = 3070$. Approximate calculations indicate that most of the discrepancy is due to the displacement effect of the boundary layer which causes the fluid in the inviscid core region to accelerate.

In the theoretical study by Kluwick & Wohlfahrt (1984), based on an integral method, the non-dimensional axial velocity profiles were expressed in the form

$$u = A(\eta_u) - f(x_0, \varphi)\, B(\eta_u), \tag{7a}$$

$$A(\eta_u) = 2\eta_u - 2\eta_u^2 + \eta_u^4, \tag{7b}$$

$$B(\eta_u) = \tfrac{1}{3}(\eta_u - 6\eta_u^3 + 8\eta_m^4 - 3\eta_u^5). \tag{7c}$$

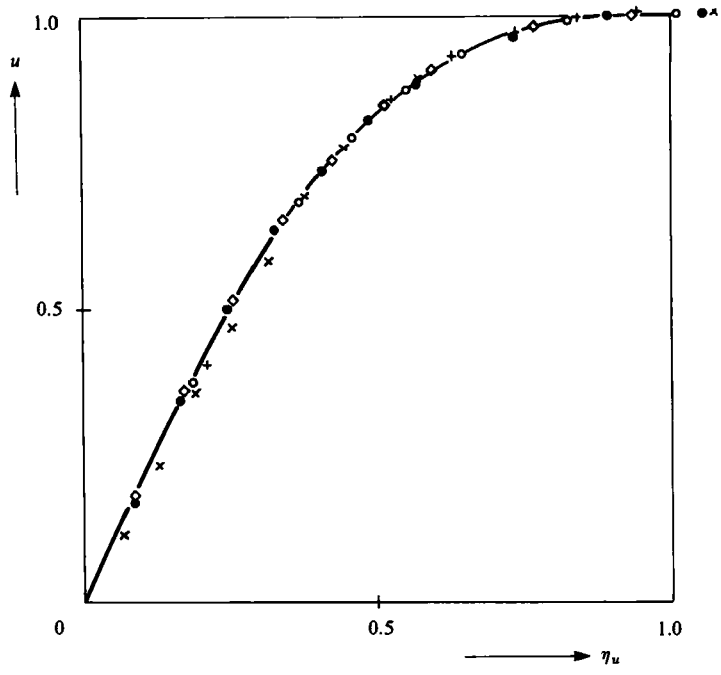

FIGURE 10. Non-dimensional streamwise velocity profiles in terms of the boundary-layer variable η_u: $\varphi = 0$, $Re = 3070$: ×, $x_0 = 0.12$; +, 0.32; ○, 0.52; ◇, 0.72; ●, 0.92.

Here

$$\eta_u = \frac{\tilde{y}}{\tilde{\delta}_u} \tag{8}$$

denotes the distance from the wall non-dimensionalized by the boundary-layer thickness $\tilde{\delta}_u$. In (7*a*), $A(\eta_u)$ represents the polynomial approximation to the Blasius profile introduced by Pohlhausen (1921).

According to the numerical results presented in Kluwick & Wohlfahrt (1984) the axial velocity profiles change only slowly with x_0 and φ except for a small area in the vicinity of the singular point which, for $K_0 = 0.1$, is located at $x_0 \approx 1.1$, $\varphi = \pi$. Furthermore, over most of the region considered in this experimental study the shape factor $f(x_0, \varphi)$ was found to be very small thus causing the theoretical profiles to collapse almost into a single curve.

Along the outer bend this result is in very good agreement with the experimental data for all test sections provided that the similarity variable $\eta_u = \tilde{y}/\tilde{\delta}_u$ is based on a boundary-layer thickness $\tilde{\delta}_{u,\mathrm{m}}$ estimated from the measured velocity profiles rather than the calculated value $\tilde{\delta}_u$ as shown in figure 10. To this end $\tilde{\delta}_{u,\mathrm{m}}$ was obtained from the distribution of the displacement thickness given in figure 9 using the approximate relationship

$$\tilde{\delta}_u^* = 0.3\, \tilde{\delta}_{u,\mathrm{m}} \tag{9}$$

which follows from (7) for small values of the shape factor $f(x_0, \varphi)$.

According to theoretical investigations (Kluwick & Wohlfahrt 1984; Stewartson *et al.* 1980; Weiss 1976) based on classical boundary-layer theory the velocity distribution along the outer bend approaches an asymptotic profile in the limit $x_0 \to \infty$. However, the numerical data indicate that the deviations from the asymptotic profile are small if $x_0 \gtrsim 1$. As mentioned earlier, the measured velocity profiles for $x_0 = 1.12$, 1.32 and 1.32 are virtually undistinguishable along $\varphi = 0$, in good agreement with

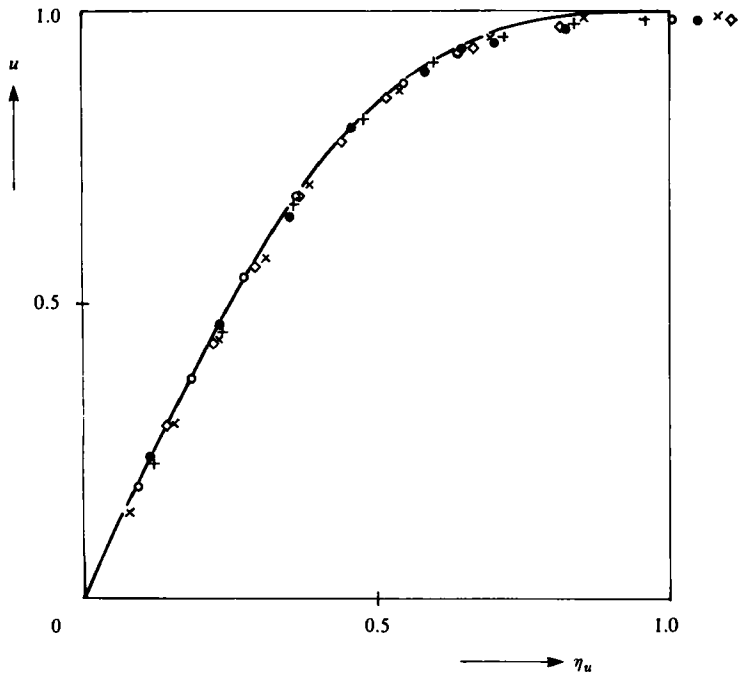

FIGURE 11. Non-dimensional streamwise velocity profiles in terms of the boundary-layer variable η_u: $\varphi = \pi$, $Re = 3070$: ×, $x_0 = 0.12$; +, 0.32; ○, 0.52; ◇, 0.72; ●, 0.92.

the theoretical result. In addition, as predicted by theory (Kluwick & Wohlfahrt 1984) the asymptotic profile differs only slightly from a Blasius profile, figure 10.

Along the inner bend the plots of u versus η_u differ only slightly from a single curve up to about $x_0 = 0.92$, see figure 11. For larger values of x_0, however, the influence of the term $f(x_0, \varphi)\, B(\eta_u)$ in (7*a*) becomes appreciable. Since the theoretical results given in Kluwick & Wohlfahrt (1984) are no longer valid as the boundary-layer singularity is approached these curves are not included in figure 11.

Finally, by extrapolating the experimental data for the streamwise velocity components down to $y = 0$ an attempt was made to estimate the position x_{0c} of the crossover point where the streamwise shear rates along the inner and outer bends coincide. While the measurements for $Re = 3070$ yield $x_{0c,m} \approx 0.70$ the values calculated in Kluwick & Wohlfahrt (1984) and Singh (1974) are $x_{0c} = 0.74$ and 0.63 respectively. However, since the minimum distance between the hot wire and the wall is about 0.3 mm, which corresponds to approximately $0.05\, \tilde{\delta}_u$ near the crossover point, the measured value $x_{0c,m}$ has to be taken with some reservation.

As already mentioned, the theoretical approach presented in Kluwick & Wohlfahrt (1984) breaks down downstream near the inner bend as well as in a small area upstream of the singularity. Numerical solutions of the first-order boundary-layer equations in the limits of infinite Dean number and $K_0 = 0$ that also included this region were obtained by Stewartson *et al.* (1980). In addition, the analytical structure of the flow near the singluarity was elucidated by Stewartson & Simpson (1982). According to these studies the streamwise component of the wall shear decreases rapidly with increasing distance from the inlet and vanishes at the location $x_0 = x_{0s}$ of the singluarity. For $x_0 > x_{0s}$ the wall shear increases again and approaches a

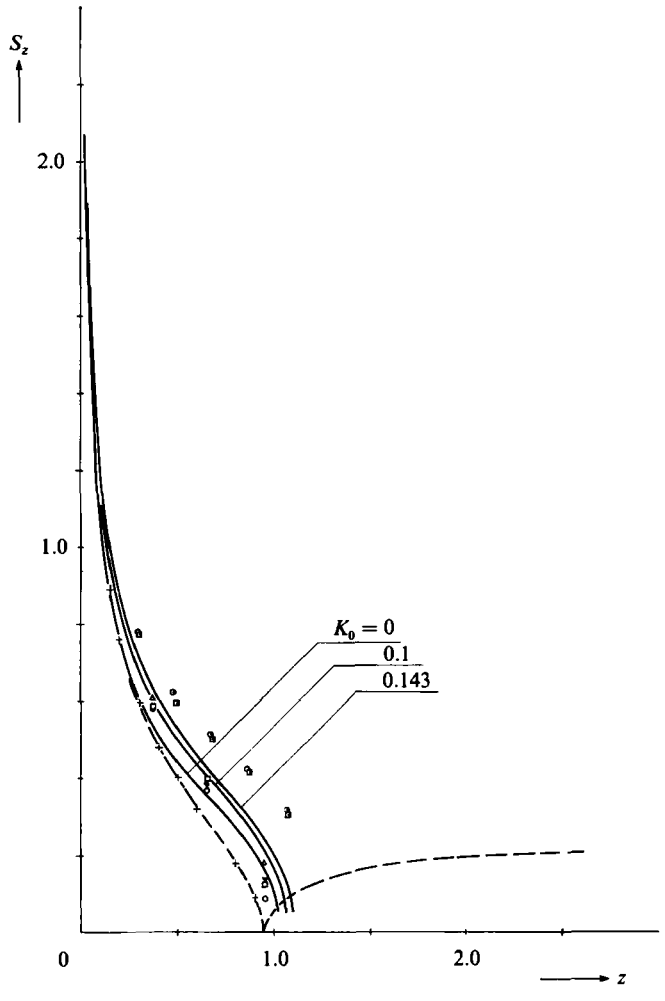

FIGURE 12. Shear-stress distribution along the inner bend: ------, Stewartson *et al.* (1980); ——, integral method (Kluwick & Wohlfahrt 1984; Wohlfahrt 1981). Talbot & Wong (1982), $K_0 = 0.143$: □, $D = 322$: △, 475; ▽, 678; ○, 811. Present measurements: ⊡, $D = 2527$; ⊙, 971.

constant value as $x_0 \to \infty$ (figure 12). Here the non-dimensional distance z and the streamwise shear rate S_z are defined as

$$z = x_0(1+K_0)^{-\frac{1}{2}}, \tag{10}$$

$$\left.\begin{aligned} S_z &= D^{-\frac{1}{2}}\left(\frac{\partial u}{\partial y}\right)_{y=0}(1+K_0\cos\varphi) \\ &= D^{-\frac{1}{2}}\frac{\tilde{\tau}_{0u}}{\tilde{\mu}}\frac{\tilde{\xi}_0}{\tilde{U}_0}(1+K_0\cos\varphi), \end{aligned}\right\} \tag{11}$$

where $\tilde{\tau}_{0u}$ denotes the component of the wall shear stress in the axial direction.

Measurements of S_z along the inner bend have recently been performed by Talbot & Wong (1982) using the electrochemical method developed in Choi *et al.* (1979). As shown in figure 12 their data are in very good agreement with the theoretical result of Stewartson *et al.* (1980) upstream of the singularity $z_s \approx 0.94$. Downstream, larger

discrepancies occur which for $z \gtrsim 2$ are 'most likely associated with a vortex structure imbedded within the Dean-type secondary motion' as discussed in Choi *et al.* (1979).

Also included in figure 12 are the experimental data obtained from the present measurements by extrapolation of the recorded velocity plots down to $y = 0$. Although these data qualitatively follow the same trend, the values of S_z are consistently higher than those obtained in Talbot & Wong (1982), the largest discrepancies occurring near the singularity found in Stewartson *et al.* (1980) from first-order boundary-layer equations in the limit of infinite Dean number and $K_0 = 0$. However, as shown in Stewartson & Simpson (1982), a two-layer structure develops inside the boundary layer as the singularity is approached from upstream. Investigation of the flow properties close to the wall reveals that the velocity gradient at the wall decreases rapidly as $z \to z_s$, which may also make it difficult to obtain accurate estimates of the wall-shear rates from velocity measurements for high-but-finite Dean numbers. The flow in the outer region reacts almost passively to these rapid changes near the wall, the oncoming boundary layer being simply lifted up and pushed away from the wall of the pipe to leading order. As already mentioned the experimental data depicted in figures 7 and 8 are not at variance with this conclusion although the structure seems to evolve at a somewhat larger distance from the inlet than predicted in Stewartson & Simpson (1982). Furthermore, figures 7 and 8 indicate that the velocity profile in the outer part of the boundary layer also remains almost unchanged downstream of the singularity up to relatively large values of x_0, in fact through the whole region considered.

7. Concluding remarks

Experiments have been performed to determine the velocity distribution inside the boundary layer and the inviscid core of a weakly curved pipe near the inlet when the incoming flow is a potential vortex. The measurements, which have been carried out up to a distance of about three pipe diameters from the entry cross-section for Dean numbers between 971 and 2527, indicate that the velocity distribution inside the boundary layer along the outer bend approaches an asymptotic profile in the limit $z \to \infty$ considered by Weiss (1976) and Stewartson *et al.* (1980). With the exception of the vicinity of the singularity, which occurs along the inner bend according to classical boundary-layer theory (Stewartson *et al.* 1980) the measured velocity profiles are in good agreement with the results derived in Kluwick & Wohlfahrt (1984) using integral relationships. Much larger discrepancies are found between predicted and measured boundary-layer thicknesses, indicating the importance of second-order boundary-layer-displacement effects.

While the velocity measurements did not allow the accurate resolution of the near-wall region developing near the singularity along the inner bend, the experimental data obtained for the outer region of the boundary layer seem to support the result given by Stewartson & Simpson (1982) that the oncoming flow there is pushed away from the wall almost passively leading to only small changes in the velocity profiles in the outer part of the boundary layer. Furthermore, this behaviour is also found downstream of the singularity where no analytical solution seems to be available at present.

REFERENCES

AGRAWAL, Y., TALBOT, L. & GONG, K. 1978 Laser anemometer study of flow development in curved circular pipes. *J. Fluid Mech.* **85**, 497–518.

BERGER, S. A., TALBOT, L. & YAO, L. S. 1983 Flow in curved pipes. *Ann. Rev. Fluid Mech.* **15**, 461–512.

CHOI, U. S., TALBOT, L. & CORNET, I. 1979 Experimental study of wall shear rates in the entry region of a curved tube. *J. Fluid Mech.* **93**, 465–489.

HOLT, M. & YEUNG, W. S. 1983 A numerical investigation for curved pipe flow at high Reynolds number. *Trans. ASME* E: *J. Appl. Mech.* **50**, 239–243.

KLUWICK, A. & WOHLFAHRT, H. 1984 Entry flow in weakly curved ducts. *Ingenieur-Archiv* **54**, 107–120.

OLSON, D. E. & SNYDER, B. 1985 The upstream scale of flow development in curved circular pipes. *J. Fluid Mech.* **150**, 139–158.

POHLHAUSEN, K. 1921 Zur näherungsweisen Integration der Differentialgleichungen der laminaren Reibungschicht. *Z. angew. Math. Mech.* **1**, 252–268.

SINGH, M. P. 1974 Entry flow in a curved pipe. *J. Fluid Mech.* **65**, 517–539.

STEWARTSON, K., CEBECI, T. & CHANG, K. C. 1980 A boundary layer collision in a curved duct. *Q. J. Mech. Appl. Math.* **33**, 59–75.

STEWARTSON, K. & SIMPSON, C. J. 1982 On a singularity initiating a boundary layer collision. *Q. J. Mech. Appl. Math.* **35**, 1–16.

TALBOT, L. & WONG, S. J. 1982 A note on boundary-layer collision in a curved pipe. *J. Fluid Mech.* **122**, 505–510.

WEISS, H. H. 1976 A contribution to the calculation of laminar boundary layers in the entrance of curved ducts. Presented at the *Euromech Colloquium 72, 30 March–1 April 1976, Salford, England.*

WOHLFAHRT, H. 1981 Theoretische und experimentelle Untersuchung der stationären laminaren inkompressiblen Strömung im Eintrittsbereich kreisförmig gekrümmter Rohre konstanten Querschnittes. Dissertation TU Vienna.

YAO, L. S. & BERGER, S. A. 1975 Entry flow in a curved pipe. *J. Fluid Mech.* **67**, 177–196.

YEUNG, W. S. 1980 Laminar Boundary Layer Flow Near the Entry of a Curved Circular Pipe. *Trans. ASME* E: *J. Appl. Mech.* **47**, 697–702.